Theory of the Tertiary Instability and the Dimits Shift from Reduced Drift-Wave Models

Hongxuan Zhu, Yao Zhou, and I. Y. Dodin

Theory of the tertiary instability and the Dimits shift from reduced drift-wave models

Hongxuan Zhu,[1,2] Yao Zhou,[1] and I. Y. Dodin[1,2]

[1]*Princeton Plasma Physics Laboratory, Princeton, NJ 08543*
[2]*Department of Astrophysical Sciences, Princeton University, Princeton, NJ 08544*

Tertiary modes in electrostatic drift-wave turbulence are localized near extrema of the zonal velocity $U(x)$ with respect to the radial coordinate x. We argue that these modes can be described as quantum harmonic oscillators with complex frequencies, so their spectrum can be readily calculated. The corresponding growth rate γ_{TI} is derived within the modified Hasegawa–Wakatani model. We show that γ_{TI} equals the primary-instability growth rate plus a term that depends on the local U''; hence, the instability threshold is shifted compared to that in homogeneous turbulence. This provides a generic explanation of the well-known yet elusive Dimits shift, which we find explicitly in the Terry–Horton limit. Linearly unstable tertiary modes either saturate due to the evolution of the zonal density or generate radially propagating structures when the shear $|U'|$ is sufficiently weakened by viscosity. The Dimits regime ends when such structures are generated continuously.

Drift-wave (DW) turbulence plays a significant role in fusion plasmas and can develop from various "primary" instabilities [1–7]. However, having their linear growth rate γ_{PI} above zero is not enough to make plasma turbulent, because the "secondary" instability can suppress turbulence by generating zonal flows (ZFs) [5–12]; hence, the threshold for the onset of turbulence is modified compared to that in the linear theory. This constitutes the so-called Dimits shift [12–17], which has been attracting attention for two decades. The finite value of the Dimits shift is commonly attributed to the "tertiary" instability (TI) [5], and some theories of the TI have been proposed [5, 15–20]. However, basic understanding and generic description of the TI and the Dimits shift have been elusive.

Here, we propose a simple yet quantitative theory of the TI using the modified Hasegawa–Wakatani equation (mHWE) [2, 16] as a base turbulence model. We clarify several misconceptions regarding the TI, and we explicitly derive the Dimits shift in the limit corresponding to the Terry–Horton model [15, 21]. Our approach is also applicable to other DW models, such as ion-temperature-gradient (ITG) turbulence [5], as discussed towards the end. Furthermore, we explain TI's role in two types of predator–prey (PP) oscillations, in determining the characteristic ZF scale in the Dimits regime, and in transition to the turbulent state.

Model equations.— The mHWE [2, 16] is a slab model of two-dimensional electrostatic turbulence with a uniform magnetic field $\boldsymbol{B} = B\hat{\boldsymbol{z}}$. Turbulence is considered on the plane (x, y), where x is the radial coordinate and y is the poloidal coordinate. The model describes φ and n, which are fluctuations of the electric potential and density, respectively. Ions are assumed cold while electrons have finite temperature T_{e}. The plasma is assumed to have an equilibrium density profile $n_0(x)$ parameterized by a constant $\kappa \doteq a/L_n$, where a is the system length and $L_n \doteq (-n_0'/n_0)^{-1}$. (We use $\doteq$ to denote definitions and prime to denote ∂_x.) Plasma resistivity produces primary instabilities and is modeled by the "adiabaticity parameter" α. We normalize time by a/C_{s} where $C_{\mathrm{s}} \doteq \sqrt{T_{\mathrm{e}}/m_{\mathrm{i}}}$,

length by $\rho_s \doteq C_{\mathrm{s}}/\Omega_{\mathrm{i}}$, where Ω_{i} is the ion gyrofrequency, φ by $T_{\mathrm{e}}\rho_{\mathrm{s}}/ea$, and n by $n_0\rho_{\mathrm{s}}/a$. Then, the mHWE is written as [16]

$$\mathrm{d}_t w = \kappa\partial_y\varphi - \hat{D}w, \quad \mathrm{d}_t n = \alpha(\tilde{\varphi} - \tilde{n}) - \kappa\partial_y\varphi - \hat{D}n. \quad (1)$$

Here, $\mathrm{d}_t \doteq \partial_t + (\hat{\boldsymbol{z}} \times \nabla\varphi) \cdot \nabla$ and $w \doteq \nabla^2\varphi - n$ is minus the ion gyrocenter-density perturbation [22]. Also, $\tilde{\varphi}$ and $\tilde{n}$ are the non-zonal parts of φ and n; e.g., $\tilde{\varphi} \doteq \varphi - \langle\varphi\rangle$, where $\langle\ldots\rangle$ denotes average over y, or zonal average. The operator $\hat{D}$ models drag and (or) viscosity; its specific form is not essential. (We choose $\hat{D}$ to be hyperviscosity large compared to that in Ref. [16], so the related effects manifest in simulations faster and more clearly.) The zonal average of Eq. (1) reads

$$\partial_t U = -\langle\tilde{v}_x\tilde{v}_y\rangle' - \hat{D}U, \quad \partial_t N = -\langle\tilde{v}_x\tilde{n}\rangle' - \hat{D}N, \quad (2)$$

where $U(x,t) \doteq \langle\varphi\rangle'$ is the ZF velocity, $N(x,t) \doteq \langle n\rangle$ is the zonal-density perturbation, and $(\tilde{v}_x, \tilde{v}_y) = \hat{\boldsymbol{z}} \times \nabla\tilde{\varphi}$. Below, we develop our TI theory based on Eq. (1). An example of mHWE simulations is also illustrated in Fig. 1 and will be discussed later.

Tertiary instability.— Absent ZFs, $w \propto e^{i(\boldsymbol{p}\cdot\boldsymbol{x}-\Omega_{\boldsymbol{p}}t)}$ is a linear eigenmode whose dispersion relation is similar to that in the Hasegawa–Mima model [1]:

$$\Omega_{\boldsymbol{p}} = \frac{\kappa p_y}{\bar{p}^2} - iD_{\boldsymbol{p}}, \quad \bar{p}^2 \doteq p_x^2 + p_y^2 + \frac{i\alpha + \kappa p_y}{i\alpha + iD_{\boldsymbol{p}} + \Omega_{\boldsymbol{p}}}. \quad (3)$$

Here, $\boldsymbol{p} = (p_x, p_y)$, and $D_{\boldsymbol{p}}$ is obtained from $\hat{D}$ by replacing ∇ with $-i\boldsymbol{p}$. The primary instability develops when $\gamma_{\mathrm{PI}} \doteq \mathrm{Im}\,\Omega_{\boldsymbol{p}} > 0$, and γ_{PI} is maximized at $p_x = 0$ and $p_y \sim 1$. However, this instability is modified once ZFs are generated by the secondary instability. In the presence of ZFs, DWs tend to localize near extrema of U, as seen in Fig. 1(a) (also observed in Refs. [3, 23, 24]), and their growth rates are also affected. To describe these effects, we assume a zonal state with prescribed $U(x)$ and $N(x)$ and consider a perturbation $\tilde{w} = \mathrm{Re}[\psi(x)e^{i(p_y y-\omega t)}]$. Then, the linearized mHWE (1) leads to

$$\omega\psi = \hat{H}\psi, \quad \hat{H}(x,\hat{p}_x) = p_y[U+(\kappa_{\mathrm{eff}}+U'')\hat{p}^{-2}]-i\hat{D}. \quad (4)$$
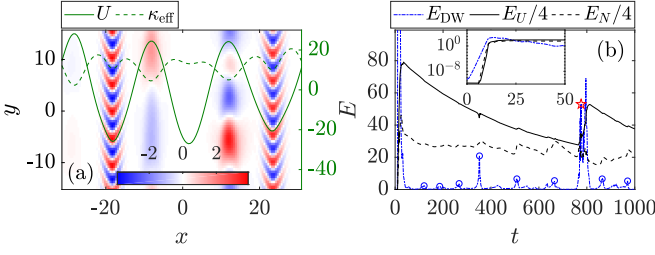
FIG. 1. Results of mHWE simluations using DEDALUS [25] with $\alpha = 5$, $\kappa = 12$, and $\hat{D} = 0.1\nabla^4$. The system is initialized with small random noise. (a) A snapshot at $t = 1000$ showing fluctuations $\tilde{w}$ (color), U (solid line), and $\kappa_{\text{eff}} \doteq \kappa - N'$ (dashed line). (b) Evolution of the DW energy $E_{\text{DW}} \doteq \int (\tilde{n}^2 + |\nabla\tilde{\varphi}|^2)d\boldsymbol{x}/2$, and the zonal energy $E_U = \int U^2 d\boldsymbol{x}/2$ and $E_N = \int N^2 d\boldsymbol{x}/2$. The inset is a zoom-in showing the energies in log scale at $0 < t < 50$, when the primary and secondary instabilities develop. Type-I PP oscillations are indicated by blue circles, and a type-II PP oscillation is indicated by the red star. (See text for more details.)

Here, $\kappa_{\text{eff}} \doteq \kappa - N'$, $\hat{p}_x \doteq -i d/dx$, and

$$\hat{\bar{p}}^2 \doteq \hat{p}_x^2 + p_y^2 + (i\alpha + i\hat{D} + \omega - p_y U)^{-1}(i\alpha + p_y\kappa_{\text{eff}}). \quad (5)$$

Note that $\hat{H}$ depends on ω through $\hat{\bar{p}}$.

To obtain preliminary understanding of these eigenmodes, we first adopt a simple zonal profile:

$$U(x) = u \cos q_{\text{Z}}x, \quad N(x) = 0, \quad (6)$$

in which case $\kappa_{\text{eff}} = \kappa$. Then, numerical eigenmodes can be found from Eq. (4) assuming periodic boundary conditions. There are infinitely many eigenmodes, but most of them are small-scale and heavily damped. The two most unstable modes have the largest scales [Fig. 2(a)]. These modes can be intuitively understood by examining their corresponding Wigner functions, $W(x, p_x) \doteq \int ds\, e^{-i p_x s}\psi(x + s/2)\psi^*(x - s/2)$, which loosely represents the distribution function of DW quanta, or "driftons" [26, 30] (the asterisk denotes complex conjugate). In large-scale ZFs, driftons obey Hamilton's equations, where the Hamiltonian H is obtained from $\hat{H}$ by replacing $(\hat{D}, \hat{p}_x)$ with $(D_{\boldsymbol{p}}, p_x)$ and taking the real part of the result [28, 30]:

$$H(x, p_x) = p_y[U + (\kappa + U'')\text{Re}\,\bar{p}^{-2}]. \quad (7)$$

Naturally, driftons tend to accumulate near phase-space equilibria of H, which are $x = x_n \doteq n\pi/q_{\text{Z}}$, $p_x = 0$ ($n = 0, \pm 1, \pm 2, \dots$), so W peaks near these locations (and overall, is aligned with isosurfaces of H), as seen in Fig. 2(b). This explains eigenmode localization near extrema of U. Maxima of U (even n) correspond to phase-space islands encircled by "trapped" trajectories, and minima (odd n) correspond to saddle points passed by the "runaway" trajectories [27–30]. Hence, we call the modes localized near maxima and minima of U as trapped and runaway modes, respectively.

Let us consider a mode localized near some $x = x_n$ and shift the origin of x, so $U \approx U_0 + \mathcal{C}x^2/2$, where $U_0 = \pm u$ is the ZF velocity at the extremum and $\mathcal{C} \doteq U''(0) = \mp q_{\text{Z}}^2 u$ is the local ZF "curvature". Since the mode is localized in both x and p_x, one can Weyl-expand [31] $\hat{H}$ as $\hat{H} \approx \mathcal{H} + \lambda_p \hat{p}_x^2 + \lambda_x x^2$, where

$$\mathcal{H} = p_y[U_0 + (\kappa + \mathcal{C})\bar{p}_0^{-2}] - iD_0, \quad \lambda_p = -p_y(\kappa + \mathcal{C})\bar{p}_0^{-4},$$

$$\lambda_x = \frac{p_y\mathcal{C}}{2}\left[1 - \frac{p_y(\kappa + \mathcal{C})(i\alpha + p_y\kappa)}{\bar{p}_0^4(i\alpha + iD_0 + \omega - p_yU_0)^2}\right],$$

$$\bar{p}_0^2 = p_y^2 + (i\alpha + p_y\kappa)/(i\alpha + iD_0 + \omega - p_yU_0),$$

and $D_0 = D_{\boldsymbol{p}}(p_x = 0)$. Then, Eq. (4) becomes similar to the equation of a quantum harmonic oscillator

$$-\lambda_p \psi'' + \lambda_x x^2\psi = (\omega - \mathcal{H})\psi, \quad (8)$$

except that its coefficients are complex. The solutions are [32]

$$\psi_m = e^{-\frac{x^2}{2\lambda}}\mathsf{H}_m(x/\sqrt{\lambda}), \quad \omega_m = \mathcal{H} + (2m + 1)\lambda_x\lambda, \quad (9)$$

where H_m denotes Hermite polynomials, $\lambda \doteq \sqrt{\lambda_p/\lambda_x}$, and $m = 0, 1, 2, \dots$. We choose the branch of the square root with $\text{Re}\,\lambda > 0$. The runaway and trapped modes shown in Fig. 2(a) correspond to $m = 0$, and for comparison, we also plot our analytic solutions (9) in the same figure. Below, we only consider modes with $m = 0$, which usually have the largest growth rates, and hence drop the subscript m. Also note that only the local ZF curvature $\mathcal{C}$ enters Eq. (8), so the ZF does not need to be sinusoidal for Eq. (9) to hold.

TI as a modified primary instability.— If $\gamma > 0$, then the eigenmode (9) grows exponentially. This is the TI. Notice that in the absence of ZFs, ω reduces to $p_y\kappa/\bar{p}_0^2 - iD_0$, which is nothing but the primary-DW eigenfrequency (3) at $p_x = 0$. Therefore, the TI eigenmode can be understood as a standing DW eigenmode modified by the ZF, and from Eq. (9), its growth rate is

$$\gamma_{\text{TI}} = \gamma_{\text{PI}} + \Delta\gamma(\mathcal{C}), \quad \Delta\gamma = \gamma_{\text{PI}}\mathcal{C}/\kappa + \text{Im}(\lambda_x\lambda). \quad (10)$$

Here, $\Delta\gamma = 0$ at $\mathcal{C} = 0$, when γ_{TI} reduces to γ_{PI}. Also, $\Delta\gamma$ depends on the sign of $\mathcal{C}$, so the trapped and runaway modes have different growth rates. Predictions from the analytic formula (10) are compared with numerical solutions of Eq. (4) in Fig. 2(c).

These results show that mode localization is a key feature of the TI. This feature is missed in some previous studies [15, 19, 20] where the TI was derived from the interaction of just four Fourier harmonics. Also, our findings challenge the popular idea that the TI is a Kelvin–Helmholtz instability (KHI) [3, 16, 20]. Specifically, the TI studied here is caused by dissipation (i.e., finite α), just like the primary instability, while the KHI is caused by strong flow shear. Therefore, unlike the KHI that develops when the ZF is too strong, the TI develops when
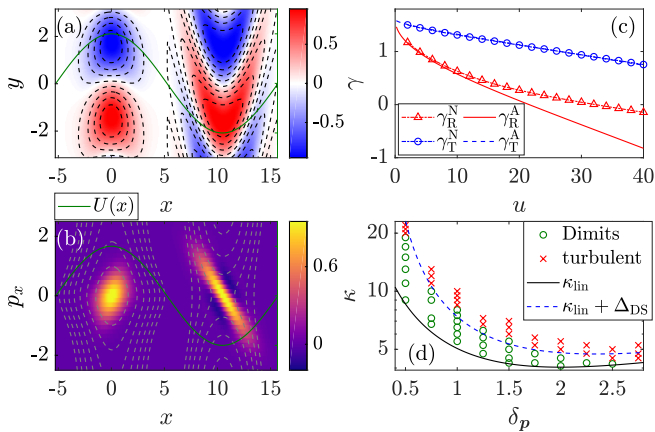
FIG. 2. (a) Trapped and runaway modes (plotted together) for the zonal profile (6): numerical solutions of Eq. (4) (color) versus analytic solutions (9) (dashed contours) at $\alpha = 5$, $\kappa = 12$, $q_Z = 0.3$, $u = 10$, and $p_y = 1$. The green curve shows U. (b) Same mode structures in phase space: Wigner functions (color) versus isosurfaces of the Hamiltonian (7) (dashed contours). (c) Numerical (labeled "N") and analytic (labeled "A") growth rates versus u. The subscripts "T" and "R" stand for "trapped" and "runaway". The analytic growth rates are obtained by solving Eq. (9) iteratively with $\omega = p_y U_0 + p_y \kappa / \bar{p}_0^2 - iD_0$ as the initial guess. (d) Dimits shift in the Terry–Horton limit: simulation results of the modified Terry–Horton equation with $\delta_{\boldsymbol{p}} = \delta_0 p_y$ and $\hat{D} = 1 - 0.01\nabla^2$ (green circles and red crosses) versus analytic results [Eq. (13) with $p_y = 1$ and $\varrho = 0.05$]. Simulation details are the same as in Ref. [15] (cf. Fig. 7 therein).

the ZF is weak and becomes suppressed when the ZF is strong. The absence of KHI is due to the fact that, in the mHWE, $\tilde{\varphi}$ is assumed to have nonzero wavenumber $p_\parallel$ along $\boldsymbol{B}$ and thus electrons respond adiabatically ($\tilde{n} \approx \tilde{\varphi}$) at large α. As shown in Ref. [33], for $\alpha \to \infty$, the KHI is suppressed at all $q_Z^2 < 1$. Here, α is finite but still large ($\alpha = 5$), so similar conclusions apply. We found numerically (not shown) that for the parameters used in Fig. 2(c), the KHI develops at $u \gtrsim 10^3$, which is too large to be relevant. Note that the assumption of nonzero $p_\parallel$ originates from the fact that the mHWE is intended to mimic turbulence in toroidal geometry with magnetic shear. But KHI can be more relevant in other geometries where $p_\parallel = 0$ is possible and electron adiabatic response does not hold [34]. For example, this is the case in Z pinches [17].

TI and Dimits shift.— The above TI theory leads to a simple understanding of the Dimits shift, at least in the large-α limit. Assuming $\omega - p_y U \approx \kappa p_y / \bar{p}^2$ and small D_0, Eq. (5) can be approximated in this limit as

$$\hat{\bar{p}}^2 = 1 + \hat{p}_x^2 + p_y^2 - i\delta_{\boldsymbol{p}}, \quad \delta_{\boldsymbol{p}} = \kappa p_y^2 / [\alpha(1 + p_y^2)]. \quad (11)$$

This corresponds to the Terry–Horton model [15, 21], which is a one-field model that evolves φ but not n (i.e., $N = 0$) and assumes a constant phase shift $\delta_{\boldsymbol{p}}$ between $\tilde{\varphi}$

and $\tilde{n}$. (Different forms of $\delta_{\boldsymbol{p}}$ can also be chosen to model different primary instabilities [15].) Then, the Hamiltonian (4) no longer depends on ω, so the growth rate is found explicitly:

$$\gamma_{\text{TI}} = \text{Im}\left[\frac{p_y(\kappa + \mathcal{C})}{1 + p_y^2 - i\delta_{\boldsymbol{p}}} \left(1 - \sqrt{\frac{\mathcal{C}}{2(\kappa + \mathcal{C})}} \right) \right] - D_0. \quad (12)$$

Here, we consider the runaway mode ($\mathcal{C} > 0$), because it is usually more unstable than the trapped mode in this model. Equation (12) allows calculation of the TI threshold, i.e., the value of κ at which $\gamma_{\text{TI}} = 0$. We denote this value as κ_c. One finds from Eq. (12) that κ_c differs from the linear threshold by Δ_{DS}:

$$\Delta_{\text{DS}} = \kappa_c - \kappa_{\text{lin}}, \quad \kappa_c = \frac{D_0}{p_y} \frac{(1 + p_y^2)^2 + \delta_{\boldsymbol{p}}^2}{\delta_{\boldsymbol{p}} - (1 + p_y^2)\sqrt{\varrho/2}}, \quad (13)$$

where $\kappa_{\text{lin}} \doteq \kappa_c|_{\varrho=0}$ is the linear threshold of the primary instability and $\varrho \doteq \mathcal{C}/\kappa$. (To simplify the formula for κ_c, we assumed the typical regime $\varrho \ll 1$.)

A ZF cannot suppress the TI at $\kappa > \kappa_c$, so Δ_{DS} is the Dimits shift. For ZFs generated self-consistently, ϱ is roughly constant (see below) and can be estimated numerically. Then, Δ_{DS} is found by minimizing Eq. (13) over p_y. Following Ref. [15], we adopt $\delta_{\boldsymbol{p}} = \delta_0 p_y$ and $\hat{D} = 1 - 0.01\nabla^2$; then, Δ_{DS} is minimized at $p_y \approx 1$ and its corresponding value is in good agreement with direct simulations of the modified Terry–Horton system [Fig. 2(d)]. The simulation details are the same as in Ref. [15], where similar numerical results are compared with a different theory. Unlike in Ref. [15], we derive Δ_{DS} explicitly and do not reduce the problem to the interaction of just four Fourier harmonics. Furthermore, our γ_{TI} is determined by the *local* ZF curvature, so Δ_{DS} is insensitive to the specific shape of the ZF.

In summary, in the Terry–Horton limit, the Dimits shift is caused by the difference between $\gamma_{\text{TI}}(\mathcal{C})$ and γ_{PI}, and the Dimits regime ends when the ZF becomes *too weak* to suppress the TI. This is different from the previous study [5] of the ITG system, which found that the TI becomes unstable when the ZF becomes too strong. The difference is due to the fact that in Ref. [5], the perturbations of the ion perpendicular temperature cause an additional destabilizing effect. However, the stabilizing effect of the ZF curvature remains the same [43].

TI's roles in nonlinear dynamics.— At smaller α, N is nonzero [35] and can affect γ_{TI} and Δ_{DS}. This makes the mHWE model more complicated than its Terry–Horton limit considered above. Nevertheless, some interesting phenomena seen in mHWE simulations can be explained in the context of our TI theory.

To simplify the mode structure, we assume large hyperviscosity, so small-scale variations of U and N are washed out. (Using normal viscosity leads to similar results, as checked numerically.) In this case, trapped and
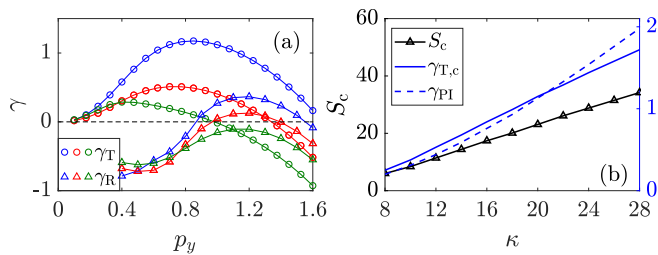
FIG. 3. (a) The growth rates of the trapped (γ_T, circles) and runaway (γ_R, triangles) modes found numerically for the zonal profile (14) at $q_Z = 0.3$ and $u = 20$. Different colors indicate different values of N_0 for trapped (runaway) modes: blue, $N_0 = 0$ ($N_0 = 0$); red, $N_0 = 5.4$ ($N_0 = 1.8$); green, $N_0 = 9$ ($N_0 = 3.6$). The peak of γ_T shifts to smaller p_y, but the peak of γ_R remains at $p_y \approx 1.2$. (b) The critical shear $S_c = q_Z u_c$ versus κ at $\alpha = 5$, $q_Z = 0.3$, and $p_y = 0.4$. We also plot γ_{PI}, and γ_T at $u = u_c$ (denoted $\gamma_{T,c}$).
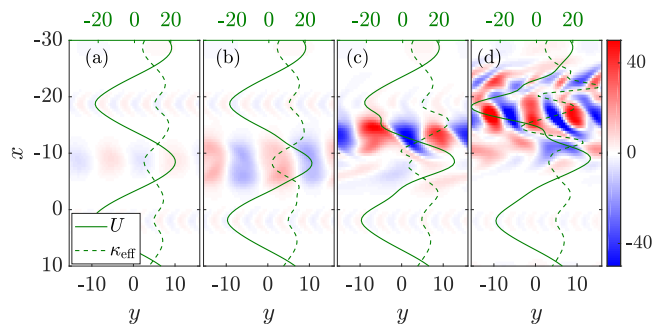

FIG. 4. Snapshots of a propagating structure corresponding to: (a) $t = 756$, (b) $t = 763$, (c) $t = 770$, and (d) $t = 777$ of Fig. 1. The axes are rotated by $90°$ compared with Fig. 1(a). This structure originates as a trapped mode ($p_y = 0.4$) at $x \approx -10$ and propagates to the neighboring minimum of U at $x \approx -20$. Both the minimum and the maximum of U are amplified by this structure, resulting in an increase of E_U.

runaway modes are still observed yet exhibit different p_y [Fig. 1(a)]. This can be explained by allowing for nonzero N. For example, we consider

$$U(x) = u \cos q_Z x, \quad N(x) = N_0 \sin 2q_Z x \qquad (14)$$

based on numerical observations [Fig. 1(a)]. The corresponding growth rates γ of the trapped and runaway modes are found numerically. It is seen in Fig. 3(a) that these growth rates decrease as N_0 increases (i.e., as κ_{eff} decreases at extrema of U). For the runaway mode, the peak of γ remains at $p_y \approx 1.2$; but for the trapped mode, the peak shifts to smaller p_y. This agrees with the self-consistent simulations showing that the trapped mode has smaller p_y [Fig. 1(a)].

Since ZFs are subject to viscous damping, turbulence cannot be suppressed indefinitely, and PP oscillations occur. Compared to those in zero-dimensional models [11], the PP oscillations are more intricate and can be of two types: type-I corresponds to the exchange between E_{DW} and E_N, while type-II corresponds to the exchange between E_{DW} and E_U [Fig. 1(b)]. Type-I PP oscillations occur more frequently because E_N decays faster than E_U (N is more prone to viscous damping due to larger wavenumber), and the corresponding bursts of E_{DW} saturate quickly due to the decrease of κ_{eff}. The latter increases E_N but has little effects on E_U, so the ZF amplitude u decreases approximately monotonically. However, when u becomes small enough, a type-II PP oscillation occurs. Then, a trapped mode does not saturate but develops into an avalanche-like nonlinear structure propagating radially (Fig. 4). This propagation triggers a turbulence burst ending with a rapid increase of the ZF amplitude; hence, E_U increases too. After such a burst, turbulence becomes suppressed again, and the Dimits regime is reinstated until the next type-II PP oscillation. (Similar propagating structures have also been found in a reduced model of ITG turbulence [36] and separately,

in simulations of DW turbulence in a linear device [37].)

Note that the propagating structures observed here are different from the DW–ZF solitons generated in the large-α limit [38]. They may be related to those seen in simulations of subcritical turbulence [39–41]. In our case, for a given q_Z, whether the trapped mode can develop into a propagating structure depends on the critical ZF amplitude u_c, or the critical shear $S_c \doteq q_Z u_c$. The critical shear in turn determines the characteristic ZF amplitude, i.e., $u \approx u_c$, because ZFs decay at $u > u_c$ and are amplified by propagating structures at $u < u_c$.

We numerically identify the critical shear by considering the initial zonal profile (6) and applying a small perturbation $\tilde{w} \propto e^{ip_y y}$. By varying u, we find the critical value $u = u_c$ and the corresponding critical shear $S_c = q_Z u_c$ above which the structure ceases to propagate. The results are shown in Fig. 3(b), where we also plot γ_{PI} and $\gamma_{T,c}$, the latter being the trapped-mode growth rate at $u = u_c$. It is seen that γ_{PI} is not a linear function of κ (rather, $\gamma \sim \kappa^{1.5}$), but both S_c and $\gamma_{T,c}$ increase linearly with κ. This justifies our earlier assumption that ϱ is constant in Eq. (13).

The effects of S (typical U') and $\mathcal{C}$ (typical U'') together determine the characteristic ZF wavenumber q_Z in the Dimits regime, specifically, as follows. First, q_Z cannot be too large, because large q_Z corresponds to small ZF amplitude $u \sim |\mathcal{C}|/q_Z^2$ assuming $|\mathcal{C}|$ is bounded by the TI threshold (otherwise, the TI is stable and the ZF decays), and ZFs with large q_Z and small u tend to merge [27, 30, 42]. Next, q_Z cannot be too small either, because small q_Z corresponds to small $|\mathcal{C}| \sim q_Z S_c$ (assuming $S \sim S_c$), unleashing the primary instability; then, the secondary instability would develop like in homogeneous turbulence and the ZF with larger q_Z would emerge.

As κ increases, the TI becomes more active in producing propagating structures. When such structures are produced almost continuously, the Dimits regime

ends, i.e., plasma becomes turbulent. As found numerically (not shown), for $\alpha = 5$, that occurs at $\kappa \gtrsim 20$. This threshold does not depend significantly on the simulation-domain size as long as the latter is large enough compared to the typical scales of ZFs and DWs.

Discussion.— Although we adopt the mHWE as our base model, our general approach to the TI is applicable more broadly. Any other model also leads to Eq. (4), except with a different $\hat{H}$. Since the TI localization is a feature common in many models [3, 5, 18, 23, 24, 36], one can Weyl-expand the corresponding $\hat{H}$ like we did above and again arrive at Eq. (9) (with different coefficients); hence, the qualitative physics remains the same. In Supplemental Material [43], we show how this approach helps reproduce the key features of the TI in ITG turbulence within the model studied in Ref. [5]. We also show there that gyrokinetic simulations of ITG turbulence (using the code GS2 [44]) exhibit similar localized modes. Although these supplemental findings are not central to our work, they suggest interesting directions for future research.

———————

[1] A. Hasegawa and K. Mima, Phys. Rev. Lett. **39**, 205 (1977).
[2] A. Hasegawa and M. Wakatani, Phys. Rev. Lett. **50**, 682 (1983).
[3] S. Kobayashi and B. N. Rogers, Phys. Plasmas **19**, 012315 (2012).
[4] W. Horton, Rev. Mod. Phys. **71**, 735 (1999).
[5] B. N. Rogers, W. Dorland, and M. Kotschenreuther, Phys. Rev. Lett. **85**, 5336 (2000).
[6] F. Jenko, W. Dorland, M. Kotschenreuther, and B. N. Rogers, Phys. Plasmas **7**, 1904 (2000).
[7] M. Leconte and R. Singh, Plasma Phys. Control. Fusion **61**, 095004 (2019).
[8] Z. Lin, T. S. Hahm, W. W. Lee, W. M. Tang, and R. B. White, Science **281**, 1835 (1998).
[9] H. Biglari, P. H. Diamond, and P. W. Terry, Phys. Fluids B: Plasma Phys. **2**, 1 (1990).
[10] P. H. Diamond, S. Champeaux, M. Malkov, A. Das, I. Gruzinov, M. N. Rosenbluth, C. Holland, B. Wecht, A. I. Smolyakov, F. L. Hinton, Z. Lin, and T. S. Hahm, Nucl. Fusion **41**, 1067 (2001).
[11] P. H. Diamond, S.-I. Itoh, K. Itoh, and T. S. Hahm, Plasma Phys. Control. Fusion **47** R35 (2005).
[12] D. R. Mikkelsen and W. Dorland, Phys. Rev. Lett. **101**, 135003 (2008).
[13] R. A. Kolesnikov and J. A. Krommes, Phys. Rev. Lett. **94**, 235002 (2005).
[14] A. M. Dimits *et al.*, Phys. Plasmas **7**, 969 (2000).
[15] D. A. St-Onge, J. Plasma Phys. **83**, 905830504 (2017).
[16] R. Numata, R. Ball, and R. L. Dewar, Phys. Plasmas **14**, 102312 (2007).
[17] P. Ricci, B. N. Rogers, and W. Dorland, Phys. Rev. Lett. **97**, 245001 (2006).
[18] B. N. Rogers and W. Dorland, Phys. Plasmas **12**, 062511 (2005).
[19] F. Rath, A. G. Peeters, R. Buchholz, S. R. Grosshauser, F. Seiferling, and A. Weikl, Phys. Plasmas **25**, 052102 (2018).
[20] E.-J. Kim and P. H. Diamond, Phys. Plasmas **9**, 4530 (2002).
[21] P. Terry and W. Horton, Phys. Fluids **25**, 491 (1982).
[22] J. A. Krommes and C.-B. Kim, Phys. Rev. E **62**, 8508 (2000).
[23] C.-B. Kim, B. Min, and C.-Y. An, Phys. Plasmas **25**, 102501 (2018).
[24] C.-B. Kim, B. Min, and C.-Y. An, Plasma Phys. Control. Fusion **61** 035002 (2019).
[25] K. J. Burns, G. M. Vasil, J. S. Oishi, D. Lecoanet, and B. P. Brown, arXiv:1905.10388. http://dedalus-project.org.
[26] A. I. Smolyakov and P. H. Diamond, Phys. Plasmas **6**, 4410 (1999).
[27] H. Zhu, Y. Zhou, and I. Y. Dodin, New J. Phys. **21**, 063009 (2019).
[28] D. E. Ruiz, J. B. Parker, E. L. Shi, and I. Y. Dodin, Phys. Plasmas **23**, 122304 (2016).
[29] H. Zhu, Y. Zhou, D. E. Ruiz, and I. Y. Dodin, Phys. Rev. E, **97**, 053210 (2018).
[30] H. Zhu, Y. Zhou, and I. Y. Dodin, Phys. Plasmas **25**, 072121 (2018).
[31] I. Y. Dodin, D. E. Ruiz, K. Yanagihara, Y. Zhou, and S. Kubo, Phys. Plasmas **26**, 072110 (2019).
[32] J. J. Sakurai, *Modern Quantum Mechanics Revised Edition*, edited by San Fu Tuan (Addison–Wesley, 1994).
[33] H. Zhu, Y. Zhou, and I. Y. Dodin, Phys. Plasmas **25**, 082121 (2018).
[34] G. W. Hammett, M. A. Beer, W. Dorland, S. C. Cowley, and S. A. Smith, Plasma Phys. Control. Fusion **35**, 973 (1993).
[35] Actually, due to nonzero N, the long-time dynamics within the mHWE model can be very different from that in the Terry–Horton or Hasegawa–Mima models even at large α. See A. J. Majda, D. Qi, and A. J. Cerfon, Phys. Plasmas **25**, 102307 (2018); D. Qi and A. J. Majda, and A. J. Cerfon, Phys. Plasmas **26**, 082303 (2019).
[36] P. G. Ivanov, A. A. Schekochihin, and W. Dorland, private communication.
[37] Y. Lang, Z. B. Guo, X. G. Wang, and B. Li, Phys. Rev. E **100**, 033212 (2019).
[38] Y. Zhou, H. Zhu, and I. Y. Dodin, Plasma Phys. Control. Fusion **61**, 075003 (2019).
[39] Y. Zhou, H. Zhu, and I. Y. Dodin, arXiv:1909.10479.
[40] F. van Wyk, E. G. Highcock, A. A. Schekochihin, C. M. Roach, A. R. Field, and W. Dorland, J. Plasma Phys. **82**, 905820609 (2016).
[41] B. F. McMillan, C. C. T. Pringle, and B. Teaca, J. Plasma Phys. **84**, 905840611 (2018).
[42] J. B. Parker and J. A Krommes, New J. Phys. **16**, 035006 (2014).
[43] See Supplemental Material at [URL will be inserted by publisher], which includes Refs. [5, 44–48].
[44] M. Barnes *et al.*, GS2 v8.0.2, https://doi.org/10.5281/

zenodo.2645150.

[45] W. D. Dorland, Ph.D. Thesis, Princeton University (1993).

[46] I. G. Abel, M. Barnes, S. C. Cowley, W. Dorland, and A. A. Schekochihin, Phys. Plasmas **15**, 122509 (2008).

[47] M. Barnes, I. G. Abel, W. Dorland, D. R. Ernst, G. W. Hammett, P. Ricci, and T. Tatsuno, Phys. Plasmas **16**, 072107 (2009).

[48] M. N. Rosenbluth and F. Hinton, Phys. Rev. Lett. **80**, 724 (1998).